

Numerical simulation of friction noise

H. Ben Abdelounis*, H. Zahouani, A. Le Bot, J. Perret-Liaudet, M. Ben Tkaya

Laboratoire de Tribologie et Dynamique des Systèmes, UMR 5513 École Centrale de Lyon, 36 avenue Guy de Collongue, 69134 Écully cedex, France

ARTICLE INFO

Article history:

Received 29 April 2010

Received in revised form 9 July 2010

Accepted 17 July 2010

Available online 3 September 2010

Keywords:

Friction noise

Roughness

Sliding contact

Dynamic

Finite element method

ABSTRACT

A numerical study to analyze friction noise being radiated when two rough and dry surfaces are rubbed together, is presented in this paper. The explicit dynamic finite element software ABAQUS in 2D is used to simulate the roughness noise. Coulomb's friction law is used at the contact surface. This simulation provided the local contact conditions such as local contact forces and contact stresses, but also the number of impacts per second and their intensities. It is shown that roughness plays a crucial role to explain roughness noise. The shocks between antagonist asperities are responsible of the transfer between the kinetic energy of solids and the vibratory energy which produces the radiation of sound. It was also shown that roughness noise level is simultaneously an increasing function of the logarithm of the surface roughness and the sliding speed. Numerical results are in agreement with our experimental results and previous studies.

© 2010 Elsevier B.V. All rights reserved.

1. Introduction

Roughness noise is the friction sound radiated when two rough surfaces are rubbed together under light normal load. Several fundamental studies on the friction noise can be found in the literature [1–5]. The most important phenomenon responsible of vibration and therefore of radiated sound is the interaction between surface roughness and waviness on the contact region of Hertzian contacts during sliding.

In addition to these theoretical studies, many experiments have been realized in order to establish the phenomenology of the friction noise [6–12]. In [11], Ben Abdelounis et al. showed that under normal light load and rough surfaces, the sliding solids are almost uncoupled and therefore the contact does not modify the natural frequencies of the sliding solids.

In this paper we present a numerical elastic model, using a transient dynamic approach, for predicting the sliding contact of rough surfaces and the roughness noise that results from this contact. The numerical approach allows us to calculate not only the level of the friction-induced vibration but also the local contact parameters such as frequency of impacts between antagonist asperities, their intensity and dissipated energy.

The model described in this paper is based on real and Gaussian topography of rough surfaces which is measured by a 2D profilometer and discretized to a finite element model.

2. Rough surface topography

The surface profiles used in this numerical simulation have been measured on real sample surfaces which have been prepared by electrical discharge machining (EDM). EDM process produces random and homogeneous surface roughness. Topographic analysis shows a Gaussian and isotropic distribution of the asperities heights. Table 1 gives the classical surface topography parameters. More details of the topography of the used surfaces are given in [11].

In Table 1, R_a is the arithmetic surface roughness, S_k and E_k are respectively the Skewness and the Kurtosis of the topography height distribution, R_{sm} is the asperities spacing, σ is the standard deviation of the asperities heights distribution, α and θ are respectively the attack angle and the apex angle such as $2\alpha + \theta = 180^\circ$ (Fig. 1).

Since the used surface profiles are Gaussians, all the classical topography parameters (R_a , σ , R_q , R_z , R_{sm}) are correlated and in particular a linear relationship is imposed between the mean arithmetic surface roughness R_a and the distance between the surface asperities R_{sm} (Fig. 2). In the following sections, both angular (attack and apex angle) and R_a parameters have been chosen to analyze our results.

3. Simulation details

3.1. Formulation problem

The two-dimensional finite element model is developed using the commercial finite element code ABAQUS/Explicit 6.7-1. The

* Corresponding author at: Laboratoire de Tribologie et Dynamique des Systèmes – Bat H10, 36 avenue Guy de Collongue 69130 Ecully, France. Tel.: +33 472186294; fax: +33 478433383.

E-mail address: houcine.ben-abdelounis@ec-lyon.fr (H. Ben Abdelounis).

Table 1
Surface roughness and topography parameters measured by profilometer on different surfaces treated by electrical discharge machining (EDM).

Electrical discharge machining (EDM)					
Ra (μm)	1	4.5	10	20	26
Sk	-0.07	-0.03	0.17	0.25	0
Ek	3.1	3.15	2.96	2.9	2.83
Rsm (μm)	92	150	276	410	516
σ (μm)	1.1	4.1	10	13	8.62
α ($^\circ$)	6.3	7.3	12.2	13	13.5
θ ($^\circ$)	167.4	165.4	155.6	154	153

explicit dynamics analysis procedure in ABAQUS/Explicit is based upon the implementation of an explicit integration rule together with the use of diagonal element mass matrices. The equation of motion is:

$$M\ddot{u}^{(i)} + F_{\text{int}}^{(i)} = F_{\text{ext}}^{(i)} \quad (1)$$

where M is the mass matrix, F_{int} is the internal force vector, F_{ext} is the applied external forces including the calculated contact forces and \ddot{u} is the acceleration such as:

$$\ddot{u}^{(i)} = M^{-1}(F_{\text{ext}}^{(i)} - F_{\text{int}}^{(i)}) \quad (2)$$

The equations of motion are integrated using the explicit central difference integration rule. The explicit central difference operator satisfies the dynamic equilibrium equations at the beginning of the increment, t ; the accelerations calculated at time t are used to advance the velocity to time $t + \Delta t/2$ and the displacement to time

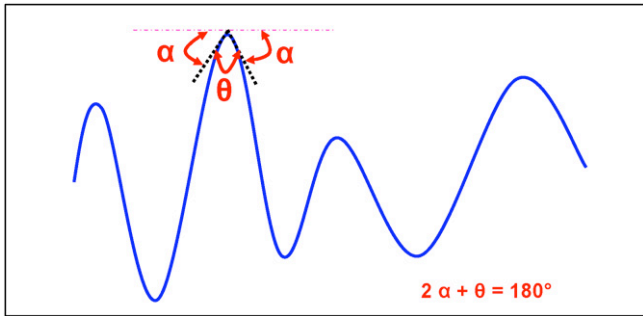


Fig. 1. Attack angle α and apex angle θ of surface asperity.

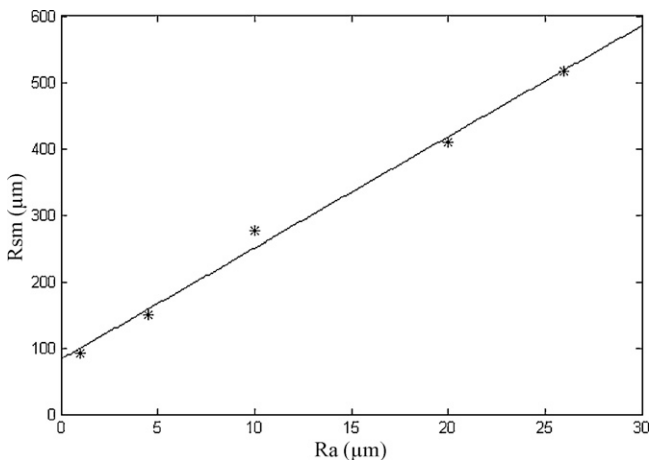


Fig. 2. Linear variation of the asperities spacing parameter Rsm versus roughness parameter Ra .

$t + \Delta t$:

$$\begin{cases} \dot{u}^{(i+1/2)} = \dot{u}^{(i-1/2)} + \frac{\Delta t^{(i+1)} + \Delta t^{(i)}}{2} \ddot{u}^{(i)} \\ u^{(i+1)} = u^{(i)} + \Delta t^{(i+1)} \dot{u}^{(i+1/2)} \end{cases} \quad (3)$$

where \dot{u} and u is the velocity and the displacement vectors and the superscript i refers to the increment number in an explicit dynamics step. It is to be noted that the explicit procedure requires no iterations and no tangent stiffness matrix.

In order to achieve stability and convergence of the central difference method, the time increment Δt must check the following condition [13]:

$$\Delta t \leq \frac{L_{\text{min}}}{c_d}$$

where L_{min} is the smallest element dimension in the mesh and $c_d \sqrt{(\lambda_0 + 2\mu_0)/\rho}$ is the dilatational wave speed of the material. λ_0 and μ_0 are the Lamé's constants and ρ is the density of the material. The stable time increment is equal to 10^{-7} s throughout this study.

3.2. Contact algorithm between deformable bodies

To determine exactly the contact parameters, such as contact forces, contact pressure, shear contact, we adopted, in our simulation the Lagrange multiplier method. The equations of this method are constructed using Eq. (1) augmented by displacement constraints acting on contacting surfaces at time $t^{(i+1)}$:

$$\begin{cases} M\ddot{u}^{(i)} + F_{\text{int}}^{(i)} + G^{(i+1)}F_c^{(i)} = F_{\text{app}}^{(i)} \\ G^{(i+1)} \{X^{(i)} + u^{i+1} - u^i\} \leq 0 \end{cases} \quad (5)$$

where $F_c^{(i)}$ is the contact force vector acting on the nodes of the slave surface, $G^{(i+1)}$ is the global assembled matrix of the constraint elementary matrices, $F_{\text{app}}^{(i)}$ is the applied external forces and $X^{(i)}$ is the vector of nodes coordinates at time $t^{(i)}$.

For this method, in each increment of the analysis, the kinematic state of the model is first advanced to a configuration predicted without considering the contact ($F_c^{(i)} = 0$). Then, the slave nodes which are penetrating the master surface are determined. The depth of each slave node's penetration, the mass associated with it, and the time increment are used to calculate the resisting force required to oppose the penetration. The next step depends on the type of master surface used. In the case of deformable bodies, the master surface is formed by element faces and the resisting forces of all the slave nodes are distributed to the nodes on the master surface. The mass of each contacting slave node is also distributed to the master surface nodes and added to their mass to determine the total inertial mass of the contacting interfaces. These distributed forces and masses are used to calculate an acceleration correction for the master surface nodes. Acceleration corrections for the slave nodes are then determined using the predicted penetration for each node, the time increment, and the acceleration corrections for the master surface nodes. These acceleration corrections are used to obtain a corrected configuration in which the contact constraints are enforced.

The friction law used here is the standard Coulomb friction model. This model assumes that no relative motion occurs if the equivalent frictional stress τ_{eq} is less than the critical stress, τ_{crit} , which is proportional to the contact pressure, P :

$$\tau_{crit} = \mu P \quad (6)$$

where μ is the friction coefficient. It was kept equal to 0.2.

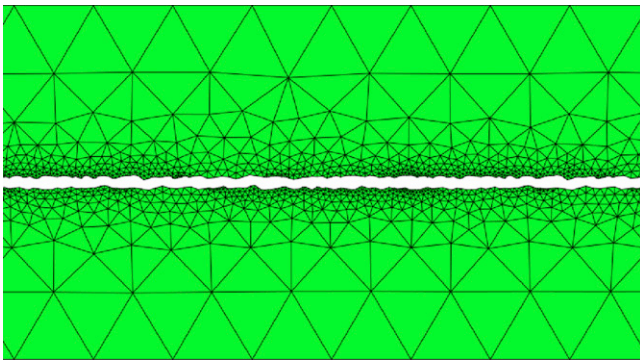


Fig. 3. Finite element mesh of 2D surface profile. The mesh is fine in contact side and coarse in back side.

3.3. Finite element model

The sliding contact between two rough solids is described using the finite elements method. For this end, a numerical dynamic model is built. The two solids have an isotropic elastic behaviour with a Young’s modulus E of 210 GPa, a Poisson’s coefficient ν of 0.3, a density ρ of 7800 kg/m³ and a structural damping of 2%.

The finite element model was based on the real topography of the rough surface. Since the used surface profiles are homogenous and isotropic, no sliding direction is preferred. In addition, the 3D model is highly time-consuming. The need to make the model as simple as possible embodies the requirement to restrict the problem to a 2D plane strain finite element model. A surface model was developed to takes into account the property of engineering surface and suitable for implementation in FE software. It aims to perform numerical analyses of the surface topography based on the real topography of the surface. The interface is presented by two elastic rough deformable surfaces in contact (120 × 8 mm²). The model was meshed by a 7764 triangular 2D plane strain element CPS3 (Fig. 3).

4. Results and discussion

The vibrational level L_v (dB) is defined as $L_v(\text{dB}) = 20 \log(V_{RMS}/V_0)$, where $V_0 = 10^{-9}$ m/s is the reference vibrational velocity of all nodes of back side, $V_{RMS}^2 = (1/N_t)(1/N) \sum_{i,j} V_{i,j}^2$

where $V_{i,j}$ is the velocity of node i at time j , N and N_t are respectively the sums of the i nodes in the back side and the j increments time.

The variation of the vibratory level L_v (dB) versus surface roughness and sliding speed is shown in Fig. 4.

From these results it is clearly seen that L_v (dB) is simultaneously a linear function of the logarithm of the surface roughness and the sliding speed according to the following relationship:

$$\Delta L_v(\text{dB}) = 20 \log \left[\left(\frac{Ra_2}{Ra_1} \right)^n \cdot \left(\frac{V_2}{V_1} \right)^m \right] \tag{7}$$

These results are in agreement with previous experimental observations [6–11]. The exponents n and m are independent and they are respectively: $0.82 \leq n \leq 0.97$ and $0.95 \leq m \leq 1.22$. To explore the effect of the amplitude and spacing roughness parameters on the friction sound, the variation of the vibratory level L_v (dB) is plotted versus (Rz/Rsm) ratio (Fig. 5). From this figure, it can be observed that the variation of the vibratory level is also a linear function of the (Rz/Rsm) ratio independently of the sliding speed in agreement

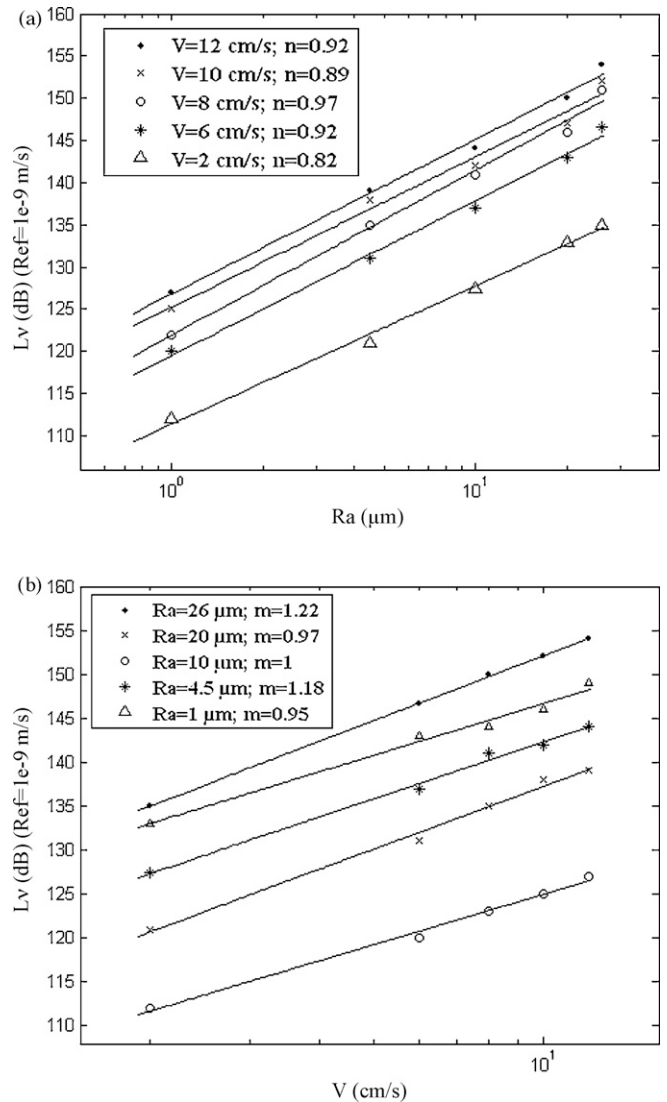


Fig. 4. Variation of the vibratory level versus (a) surface roughness and (b) sliding speed.

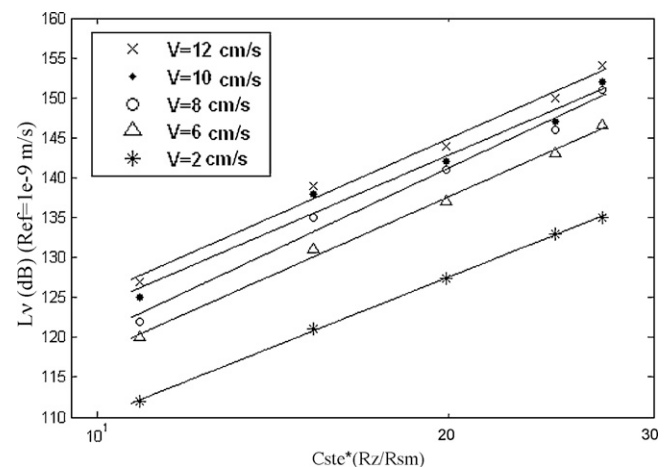


Fig. 5. Variation of the vibratory level L_v (dB) versus (Rz/Rsm) for various sliding speed.

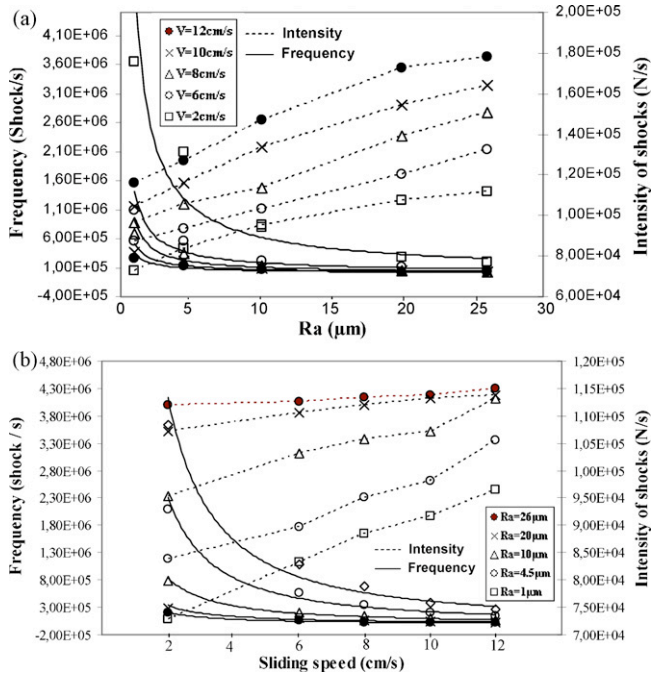


Fig. 6. Frequency and intensity of shocks versus (a) surface roughness and (b) sliding speed.

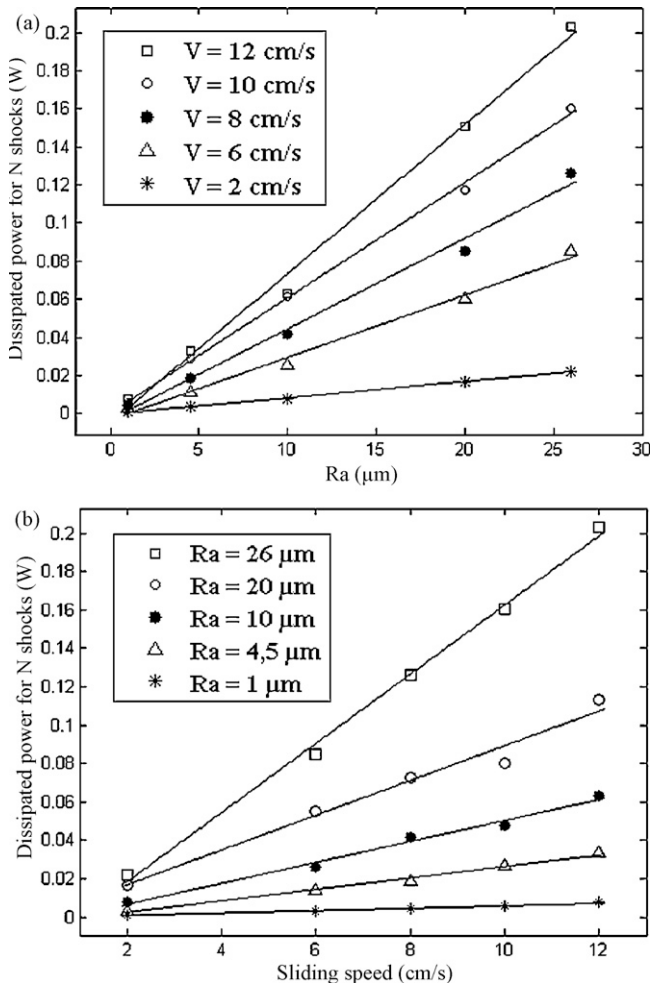


Fig. 7. Dissipated vibratory power versus (a) surface roughness and (b) sliding speed.

with the following logarithmic equation:

$$\Delta Lv(\text{dB}) = 20 \log \left(\frac{Rz}{Rsm} \right)^a \quad (8)$$

where a is a constant.

Indeed, in the case of sliding contact between rough surfaces, the sound is produced by numerous impacts between antagonist asperities. If moreover the applied load is weak, the shocks between antagonist asperities deform elastically the asperities in contact and therefore normal random contact vibrations are generated. The most important source of the energy dissipation, which a share is radiated in the acoustic energy form, is the normal vibrations excited by the irregularities of the sliding surfaces [3].

The variation of friction-induced vibration versus roughness and sliding speed is controlled by the frequency of shocks, between antagonist asperities surfaces, and their intensity. Both for increasing surface roughness and sliding speed, the frequency of shocks decreases, but their total intensity per unit time increases (Fig. 6), leading to a greater dissipated vibratory power (Fig. 7), and therefore to a higher radiated noise.

Fig. 7 shows that the dissipated vibratory power P (W) for N shocks is proportional to the surface roughness Ra (μm) and the sliding speed. As, the vibratory dissipated power is proportional to the vibratory level Lv (dB), the results of Fig. 7 are in agreement with the results presented in Fig. 4 (Lv (dB) $\propto \log P(W) \propto \log(Ra^n \cdot V^m) \propto \log(n_c * E)$, where n_c (shock/s) is the frequency shocks and E is the dissipated energy (J)).

5. Conclusions

The numerical model used in this study shows that the vibratory level Lv (dB) is a linear increasing function of the logarithm of the surface roughness and the sliding speed in agreement with our experimental results [11] and previous studies [6–10]. It is concluded also that for sliding rough surfaces under light load the fundamental mechanism of roughness noise, is the presence of shocks occurring between antagonist asperities of sliding surfaces.

References

- [1] A. Soom, C. Kim, Roughness-induced dynamic loading at dry and boundary lubricated sliding contact, *Trans. ASME J. Lub. Technol.* 105 (1983) 514–517.
- [2] A. Anand, A. Soom, Roughness-induced transient loading at a sliding contact during start-up, *Trans. ASME J. Tribol.* 106 (1984) 49–53.
- [3] A. Soom, J.W. Chen, Simulation of random surface roughness-induced contact at Hertzian contacts during steady sliding, *J. Tribol.* 108 (1986) 108–123.
- [4] A. Soom, C. Wang, Interpretation of Rubbing Noise from a Pin-On-Disc Configuration, ASME, Boston, MA, 1983, November.
- [5] D.P. Hess, A. Soom, Normal and angular motions at rough planar contacts during sliding with friction, *J. Tribol.* 114 (1992) 567–578.
- [6] K. Takashi, The friction noise under heavy load, *Bull. FAC. Sci. Eng., Chuo Univ.* 16 (1973) 53–69.
- [7] M. Nakai, M. Yokoi, A fundamental study on frictional noise (5th report, the influence of random surface roughness on frictional noise), *Bull. JSME* 25 (1982) 827–833.
- [8] M.O. Othman, A.H. Elkholy, Surfaces roughness measuring using dry friction noise, *Exp. Mech.* 47 (1990) 309–312.
- [9] M.O. Othman, A.H. Elkholy, A.A. Seireg, Experimental investigation of frictional noise and surface-roughness characteristics, *Exp. Mech.* 47 (1990) 328–331.
- [10] B.L. Stoimenov, S. Maruyama, K. Adashi, K. Kato, The roughness effect on the frequency of frictional sound, *Tribol. Int.* 40 (2007) 659–664.
- [11] H. Ben Abdelounis, A. Le Bot, J. Perret Liaudet, H. Zahouani, An experimental study on roughness noise of dry rough flat surfaces, *Wear* 268 (2010) 335–345.
- [12] A. Le Bot, E. Bou Chakra, Measurement of friction noise versus contact area of rough surfaces weakly loaded, *Tribol. Lett.* 37 (2010) 273–281.
- [13] ABAQUS, Theory and Users Manual, Version 6.7-1, Pawtucket, Rhode Island, Habbt, Karlsson and Sorensen Inc., 2007.